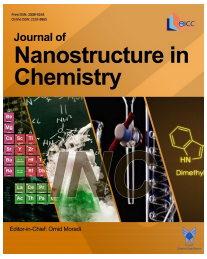

Volume 15, Issue 3, 152510 (1-10)

Journal of Nanostructure in Chemistry (JNSC)

https://doi.org/10.57647/jnsc.2025.1503.10

Fe_3O_4/RGO-Ionic liquid Nanocatalyst as Amplifier for Fabrication of Highly Sensitive Electrochemical Sensor in Monitoring of Thallium Environmental Fluids

Somaye Cheraghi[1,*], Mohammad Amin Dasar[2], Mohammad Ali Taher[2]

[1]*Department of Chemistry, University of Jiroft, Jiroft, Iran.*
[2]*Department of Chemistry, Shahid Bahonar University of Kerman, Kerman, Iran.*

[*]**Corresponding author:** chr.somaye@gmail.com

Original Research

Received:
8 March 2025
Revised:
12 May 2025
Accepted:
25 May 2025
Published online:
18 June 2025

Abstract:

The analysis of Tl(I) is essential due to its high toxicity, environmental persistence, and potential to cause neurotoxic and carcinogenic effects even at trace levels. In this work, a reduced graphene oxide–magnetite nanocomposite (rGO–Fe_3O_4) combined with the ionic liquid N -butyl-3-methylimidazolium tetrafluoroborate (N-B-3-MITFB) was used to modify a carbon paste electrode. The resulting rGO–Fe_3O_4/N-B-3-MITFB/CPE was employed for the sensitive detection of Tl(I) in aqueous samples. The electrochemical characteristics of the sensor were systematically investigated using differential pulse anodic stripping voltammetry (DPASV). This electrode demonstrated strong oxidative activity for Tl(I) at a lower overvoltage (compared to unmodified electrodes), along with a higher current response and enhanced sensitivity. Under optimal conditions (pH 7, accumulation time 400 s, scan rate of 30 mV/s), the calibration curve for Tl(I) exhibited a linear range of $0.07 - 420$ µM with a limit of detection (LOD) of 0.9 nM. The proposed sensor displayed excellent selectivity for determining Tl(I) levels in the presence of common interfering species (e.g., Pb^{2+}, Cr^{2+}, Cu^{2+}, NO_3^-). The rGO-Fe_3O_4/N-B-3-MITFB/CPE showed high analytical performance for Tl(I) analysis in diverse water samples (e.g.,drinking water, well water, and waste water), achieving recoveries of $97.5 - 102.4$%.

Keywords: Tl(I); N-butyl-3-methylimidazolium tetrafluoroborate; Reduced graphene oxide; Anodic stripping voltammetry; Modified electrode

Cite this article: Cheraghi, S., Dasar, M.A., Taher, M.A. Fe_3O_4/RGO-Ionic liquid Nanocatalyst as Amplifier for Fabrication of Highly Sensitive Electrochemical Sensor in Monitoring of Thallium Environmental Fluids. *J Nanostruct Chem* **15**(3), 152510 (2025).

1. Introduction

From a biological perspective, monovalent thallium (Tl^+) compounds are highly toxic and readily absorbable through the skin [1]. This element is relatively rare in the Earth's crust and is typically found in small quantities in minerals such as crookesite, lorandite, and hutchinsonite [2]. Thallium exhibits a distinctive set of physical and chemical characteristics, notably its high electrical conductivity and low melting point, which have historically contributed to its utilization across a broad spectrum of industrial applications, including electronics, optical systems, and even pest control as a rodenticide [3]. However, its extreme toxicity to humans and the environment has led to significant restrictions on its use [4]. The lethal dose of thallium in humans is $8 - 12$ mg/kg [5]. Additionally, Tl^+ can replace K^+ in the activation of certain enzymes, such as adenosine triphosphatase. The toxicity of Tl(I) to the biosphere is even greater than that of elements like Hg, Cd, Pb, and Cu [6, 7]. The growing concern over Tl(I) contamination in the environment, particularly in soil and water, has made reliable methods for its detection and quantification essential. The importance of measuring trace amounts of Tl(I) has led to the development of various methods, including optical emission spectrometry (OES) [8], X-ray fluorescence (XRF) [9], inductively coupled plasma mass spectrometry (ICP-MS) [10, 11], chromatography [12], and electrochemical techniques [13–16]. Since measuring very low concentrations of Tl(I) often requires a pre-concentration step, stripping voltammetry methods can be particularly useful [13, 17]. The advancement of sophisticated analytical methods con-

tinues to play a critical role in addressing the challenges associated with Tl(I) detection, thereby ensuring better protection of human health and the environment from its detrimental impacts.

Differential pulse anodic stripping voltammetry (DPASV) is a highly sensitive electrochemical technique that has gained significant attention for the detection and measurement of trace metals and other electroactive species in various matrices [18–20]. This method is especially useful in environmental monitoring, clinical diagnostics, and industrial quality control, where precise measuremet of low analyte concentrations is essential [21]. DPASV operates on the principle of concentrating the target analyte onto the electrode surface through electrodeposition, followed by subsequent oxidative stripping. This method exhibits high sensitivity as a result of the reduction in capacitive current and the enhancement of faradaic current [22, 23]. This approach has a detection limit in the nanomolar range, making it well suited for quantitative analysis and the detection of metals at low concentrations [24]. The sensitivity of this technique is attributed to the pre-concentration step, which amplifies the signal by accumulating the analyte on the electrode surface [25].

The integration of DPASV as a highly sensitive electrochemical technique with modified electrodes has revolutionized the detection and quantification of trace analytes [26, 27]. The sensitivity, stability, and selectivity of electrodes have been greatly enhanced by the introduction of materials like ionic liquids and nanomaterials, allowing for precise measurements at incredibly low concentrations [28–30]. Among these materials, graphene has attracted significant interest because of its outstanding ability to conduct electricity, expansive surface area, and remarkable durability [31–33]. For instance, Graphene oxide-magnetite nanocomposites, can be made by doping graphene with iron. These nanocomposites have better electrocatalytic qualities and perform better in electrochemical sensing [34–36].

Ionic liquids improve the performance of electrodes in voltammetry method by enhancing ion transport and reducing electrical resistance [37–39]. The use of imidazolium-based ionic liquids in combination with nanomaterials has led to increased sensitivity and stability of electrodes in the detection of heavy metals. It also enables the measurement of electroactive compounds in various matrices [40, 41]. In this work, a carbon paste electrode modified with an rGO–Fe_3O_4 nanocomposite and the ionic liquid N-B-3-MITFB was developed for the electrochemical detection of Tl(I) in aqueous samples. The simultaneous use of Fe_3O_4 nanoparticles, reduced graphene oxide, and ionic liquid for Tl(I) recognition had not been reported previously. This configuration enhanced catalytic activity and improved electron transfer. Compared to earlier studies, including those cited in [13] and [28], the proposed sensor achieved a lower detection limit, attributed to the innovative integration of nanomaterials and their synergistic effects. Furthermore, it demonstrated higher precision and better reproducibility than the method described in [42], confirming its superior reliability for practical applications.

2. Materials and methods

2.1 Chemical and Apparatus

Graphite powder (< 50 μm), phosphoric acid, ionic liquid N-Butyl-3-Methylimidazolium Tetrafluoroborate, and liquid paraffin, which were used in this study, were procured from Sigma-Aldrich. Reduced graphene oxide-iron oxide nanoparticles (rGO-Fe_3O_4 NPs) were synthesized following the procedure outlined in our previously published article [42]. The synthesis of rGO-Fe_3O_4 NPs involved materials such as, sodium hydroxide, iron (II) chloride, iron (III) chloride, potassium permanganate all of which were obtained from Merck. A Tl(I) standard solution (1000.0 mg/L) was also purchased from Merck and diluted with deionized water to prepare various concentrations of thallium solutions. Buffer solutions with pH values ranging from 3.0 to 8.0 were formulated by combining phosphoric acid with sodium hydroxide. Electrochemical experiments were performed using a Metrohm potentiostat equipped with a three-electrode configuration. The setup comprised a platinum wire as the auxiliary electrode, an Ag/AgCl electrode as the reference, and carbon paste electrodes (CPEs), either modified or bare, acting as the working electrode. All measurements were carried out under ambient temperature conditions.

2.2 Synthesis of rGO–Fe_3O_4

To synthesize the rGO–Fe_3O_4 nanocomposite, 1.08 g of $FeCl_3{\cdot}6H_2O$ and 0.39 g of $FeCl_2{\cdot}4H_2O$ were dissolved in an Erlenmeyer flask containing 100 mL of distilled water. Subsequently, 50 mL of a reduced graphene oxide (rGO) suspension (0.4 mg/mL concentration), prepared by ultrasonication of graphene oxide (GO) synthesized via Hummers' method [43], was added to the aforementioned solution under vigorous stirring. The mixture was continuously stirred for 20 minutes, after which the pH was brought to 10 by adding 0.1 M sodium hydroxide. Stirring was continued for a further 40 minutes at room temperature. The resulting black precipitate was collected using a magnet, thoroughly rinsed with deionized water several times, and subsequently dried in a controlled-temperature oven at 65 °C for 36 hours.

2.3 Preparation of rGO-Fe_3O_4/N-B-3-MITFB/CPE

To fabricate the carbon paste electrode, 0.95 g of graphite powder (as the main conductive material), 0.05 g of rGO-Fe_3O_4 nanoparticles (to enhance electrochemical activity), and 0.88 g of solid paraffin (as a binder) were thoroughly mixed in a porcelain mortar. Subsequently, 0.12 g of an ionic liquid was added to the mixture to improve ionic conductivity and enhance the stability and homogeneity of the paste. The mixture was manually ground and homogenized for approximately 30 minutes to obtain a uniform and cohesive paste. The prepared paste was then transferred into a glass tube of appropriate diameter. For establishing electrical contact, a copper wire was inserted into the tube and positioned in direct contact with the paste.

2.4 Real sample preparation

Three different water sources were selected for analysis: well water from Shahid Bahonar University of Kerman (Kerman, Iran), industrial wastewater from a copper factory in Sarcheshmeh (Kerman, Iran), and municipal drinking water from Kerman city. To remove suspended solids, the samples were filtered and subsequently stored at 4 °C. Before analysis, the pH of each sample was adjusted to 7.0 to facilitate the application of the proposed method for the detection and quantification of Tl(I).

2.5 General procedure

The determination of Tl(I) ions was performed using differential pulse anodic stripping voltammetry (DPASV) following this protocol: During the preconcentration phase, the rGO-Fe_3O_4/N-B-3-MITFB/CPE electrode was immersed in a 25.0 mL of 0.01 mol/L phosphate buffer solution (pH 7.0) containing a known concentration of Tl(I) ions, under continuous stirring for 6 minutes. In this step, Tl(I) ions were deposited onto the electrode surface by applying a potential of -0.1 V. After accumulation, voltammograms were recorded by sweeping the potential from -0.1 V to $+0.1$ V using a scan rate of 30 mV/s, a pulse amplitude of 100 mV, and a pulse duration of 4 ms. All electrochemical measurements were conducted at ambient temperature (23 ± 1 °C).

2.6 Working principle

The basis of the proposed method involves the adsorption of Tl(I) ions onto the proposed electrode. When a potential of -1.0 V is applied, Tl(I) ions present in the solution are attracted to the surface of the electrode, where they undergo preconcentration through adsorption. The Tl^+ ions collected on the electrode surface are immediately reduced to Tl^0, forming a thin metallic layer on the electrode surface. These steps are shown in the following equations:

$$Tl^+_{aq} + MCPE_{surf} \rightarrow [Tl\text{-}MCPE]_{surf} \quad (1)$$

$$[Tl\text{-}MCPE]_{surf} + e + H^+ \rightarrow Tl^0_{surf} + MCPE\text{-}H_{surf} \quad (2)$$

In the next step, the electrode surface is stripped by potential scanning from -1 to $+1$ volt through the conversion of Tl^0 to Tl^+, which leads to an analytical voltammogram

$$Tl^0_{surf} \rightarrow Tl^+_{aq} + e \quad (3)$$

peak.

In these equations, the subscripts 'aq' and 'surf' are used to signify that the compound is present in the aqueous phase or on the electrode surface, respectively.

3. Results and discussion

3.1 Characterization of rGO–Fe_3O_4 nanocomposite

The crystalline structure and particle size of the rGO-Fe_3O_4 nanocomposite were investigated using X-ray diffraction (XRD) in the 2θ angle range of 10° to 90° (Fig. 1). The diffraction peak observed at $2\theta = 12°$ corresponds to the (200) crystalline plane of graphene oxide. The low intensity of this peak indicates a significant reduction of graphene oxide to reduced graphene oxide (rGO) during the synthesis process. In addition, the diffraction peaks corresponding to the Miller indices (220), (311), (400), (422), (511), (440), (620), and (533) are characteristic of the cubic spinel structure of magnetite (Fe_3O_4), which confirms the presence of a pure and uniform magnetite phase within the nanocomposite. The approximate size of the magnetite nanoparticles was calculated to be about 23 nm using the Scherrer equation ($D = K\lambda/\beta\cos\theta$), based on the strongest diffraction peak associated with the (311) crystal plane.

FT-IR spectroscopy confirmed the reduction of graphene oxide (GO) to reduced graphene oxide (rGO) and the successful synthesis of the rGO-Fe_3O_4 nanocomposite through comparative spectral analysis. The FT-IR spectrum of pristine GO (Fig. 2) showed characteristic peaks of an oxidized structure: A broad O–H stretch (32003500 cm^{-1}), a strong C=O stretch (1720 cm^{-1}), and peaks for C=C (1620 cm^{-1}), O-H bend (1390 cm^{-1}), C-OH (1220 cm^{-1}), and C-O (1050 cm^{-1}) vibrations, indicating extensive functionalization [44]. In contrast, the rGO-Fe_3O_4 composite spectrum displayed significant changes (Fig. 3). The C=O peak (1720 cm^{-1}) and O-H band ($3200 - 3500$ cm^{-1}) markedly decreased, confirming the removal of carboxyl/carbonyl groups and partial deoxygenation. The decrease in the intensity of the C=C peak indicates that magnetite nanoparticles

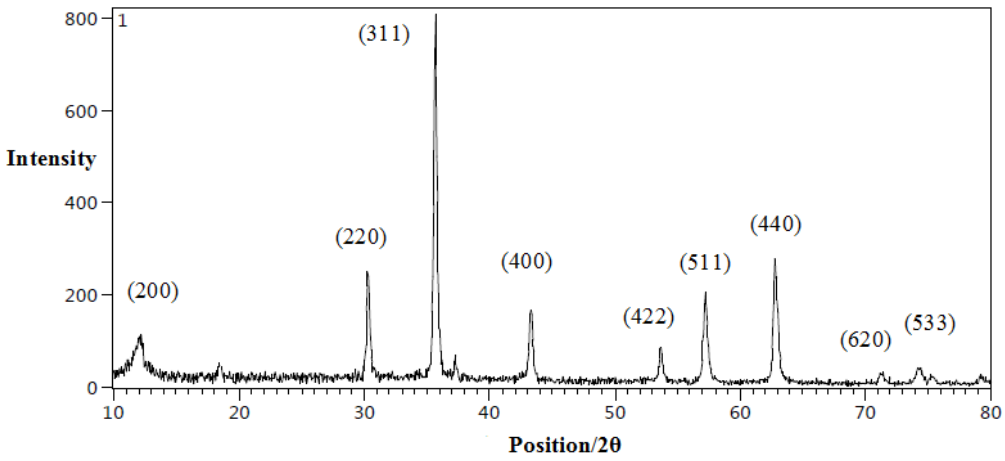

Figure 1. Powder X-ray diffraction pattern of rGO-Fe_3O_4 nanocomposite.

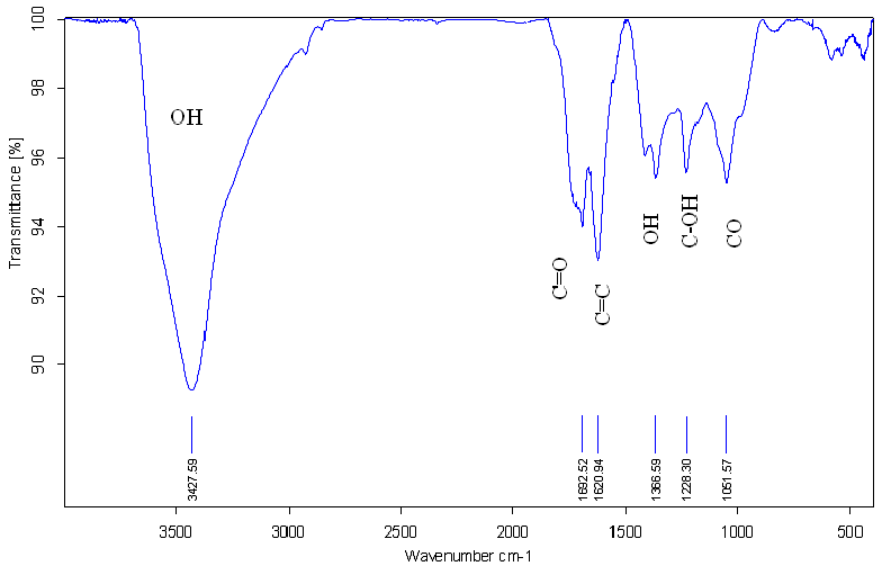

Figure 2. FT-IR spectrum of GO.

have been uniformly deposited across the entire surface of rGO. Epoxy/alkoxy peaks (1220, 1050 cm^{-1}) were also reduced, though some C-O and O-H functionalities remained, essential for nanoparticle anchoring. Distinct Fe_3O_4 peaks appeared at 584 cm^{-1}, corresponding to Fe-O vibrations in tetrahedral and octahedral sites, respectively, confirming successful nanoparticle incorporation [45]. In summary, the comparative FT-IR analysis demonstrates effective GO reduction and confirms the formation of the rGO-Fe_3O_4 nanocomposite through the significant decrease of GO's oxygen-related peaks and the emergence of Fe_3O_4 characteristic vibrations.

Field emission scanning electron microscopy (FESEM) was utilized to investigate the surface morphology of the nanocomposite (Fig. 4 A). The micrographs clearly revealed the preserved layered structure of reduced graphene oxide (rGO), the flat surfaces of the composite sheets, and the spherical-shaped Fe_3O_4 nanoparticles. The rGO layers act as a three-dimensional matrix, on which the Fe_3O_4 nanoparticles are uniformly and regularly deposited. In comparison to pristine rGO (Fig. 4 B), the FESEM images demonstrate successful decoration of the rGO sheets with Fe_3O_4 nanoparticles without significant disruption of the underlying graphene structure.

Fig. 5 (A) presents the Energy Dispersive X-ray Spectroscopy (EDS) spectrum of the rGO/Fe_3O_4 nanocomposite, clearly confirming the presence of carbon (C), oxygen (O), and iron (Fe) elements. Fig. 5 (B) shows the EDS mapping, which further reveals the spatial distribution of these key elements with high precision. The even distribution of the carbon element across the surface suggests a widespread and uniform dispersion of reduced graphene oxide (rGO) throughout the nanocomposite matrix. Signals corresponding to iron and oxygen appear as dispersed and overlap-

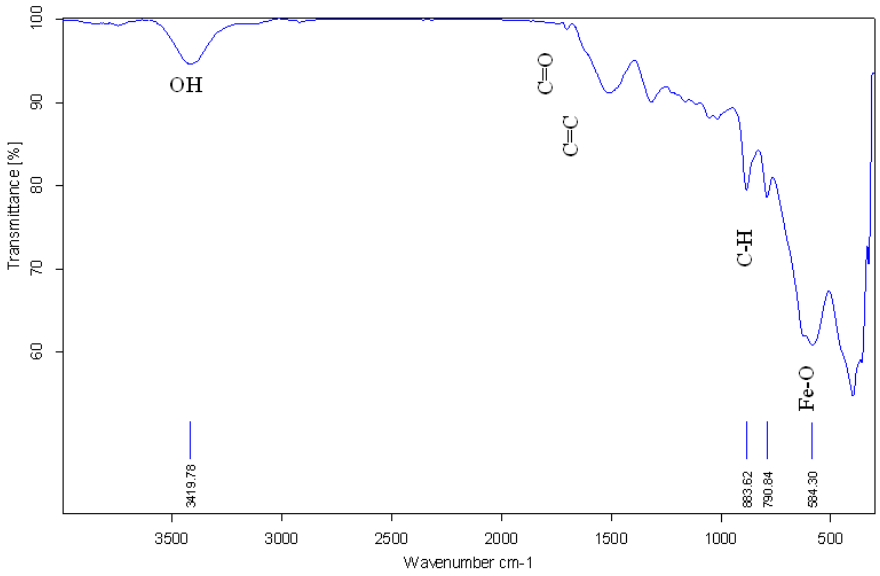

Figure 3. FT-IR spectrum of rGO-Fe_3O_4 nanocomposite.

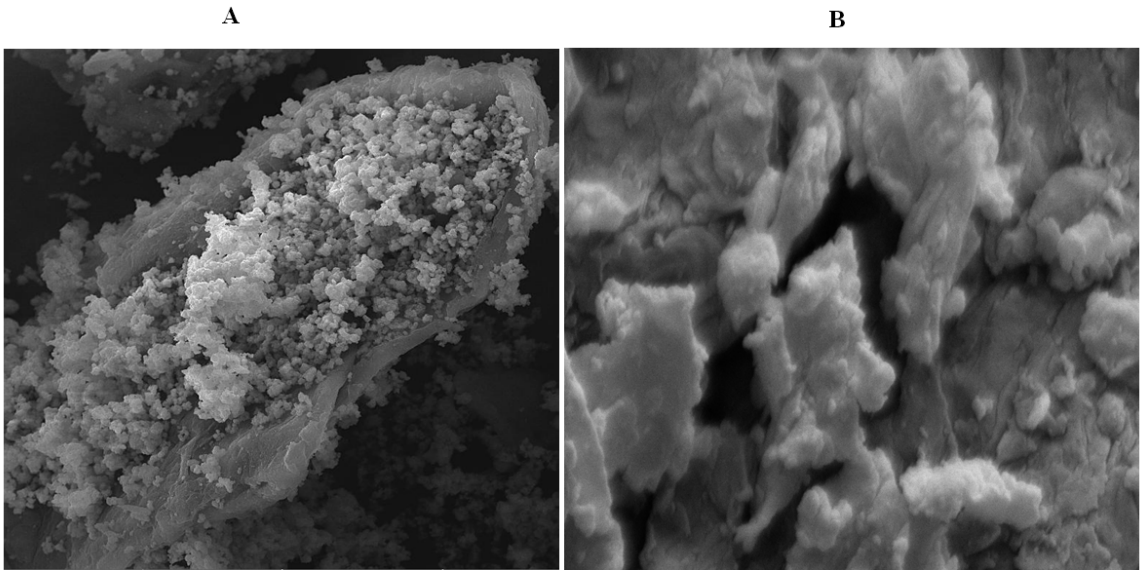

Figure 4. FESEM images of synthesized rGO-Fe_3O_4 nanocomposite (A) and rGO (B).

ping spots, indicating the effective formation of iron oxide (Fe_3O_4) nanoparticles on the rGO surface. The relatively uniform distribution of these nanoparticles, along with the absence of significant agglomeration, suggests an effective and well-controlled synthesis of the nanostructured composite.

The BET method is a widely used technique for determining the specific surface area of porous materials (Fig. 6 A). BET analysis of the synthesized rGO-Fe_3O_4 nanocomposite revealed a specific surface area of 210 m^2/g, indicating of substantial porosity and a high degree of surface accessibility, which are often associated with enhanced adsorption and catalytic properties. The BJH method (Fig. 6 B), commonly applied to assess pore size distribution and pore volume in mesoporous materials, showed an average pore size of 1.86 nm and an average pore volume of 0.1704 cm^3/g.

3.2 Electrochemical behavior of rGO-Fe_3O_4/N-B-3-MITFB/CPE

The preconcentration capability of the modified carbon paste electrode for Tl(I) was evaluated. Differential pulse voltammograms were recorded for various electrode modifications in the presence of 300 μM Tl(I): Unmodified carbon paste (b), modified with rGO-Fe_3O_4 nanocomposite (c), modified with ionic liquid (d), and modified with both rGO-Fe_3O_4 nanocomposite and ionic liquid (e). A voltammogram was also obtained for the combined rGO-Fe_3O_4/ionic liquid modified electrode in the absence of Tl(I) (a), (Fig. 7). The highest Tl(I) oxidation current was observed with the electrode modified with both rGO-Fe_3O_4

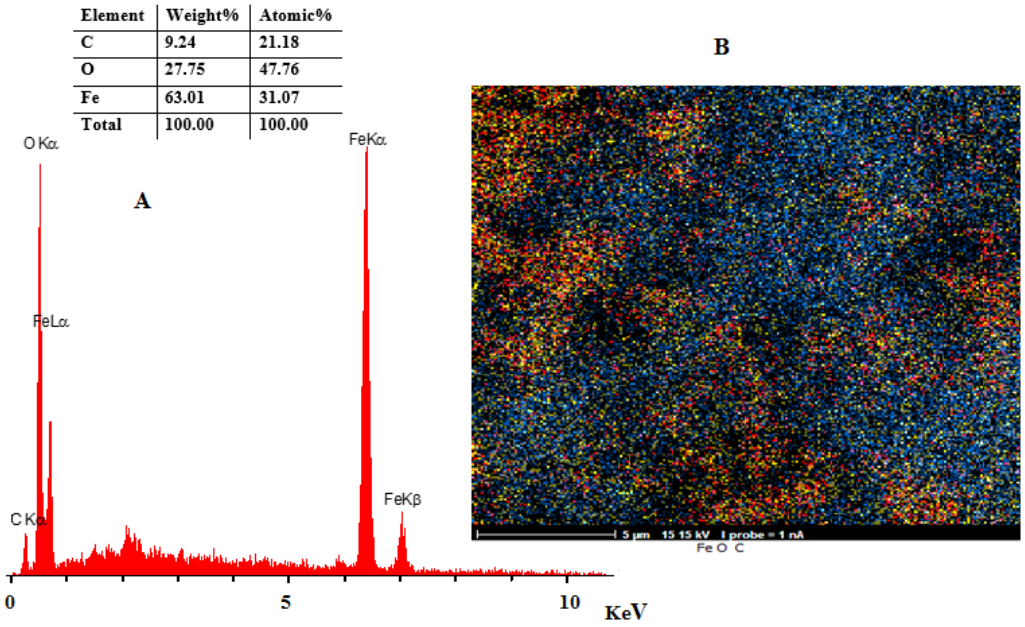

Figure 5. EDS patterns (A) and EDS mapping (B) of rGO-Fe_3O_4 nanocomposite.

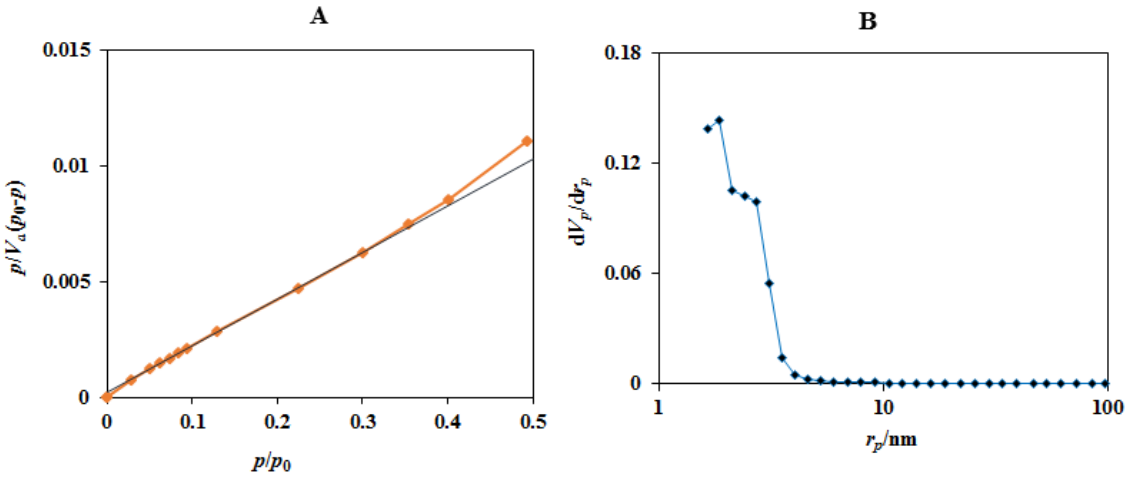

Figure 6. BET (A) and BJH (B) analysis of rGO-Fe_3O_4 nanocomposite.

nanocomposite and ionic liquid, indicating superior performance. This enhanced current is attributed to the modifiers, which increase the electrode's active surface area (leading to greater Tl(I) adsorption), improve conductivity, facilitate enhanced electron transfer through the synergistic effects of rGO ionic liquid, and Fe_3O_4, and potentially provide catalytic sites for the Tl(I) oxidation process. Therefore, both the ionic liquid and the rGO-Fe_3O_4 nanoparticles are crucial for effective Tl(I) detection.

3.3 Electrochemical impedance study

The electro-oxidation of Tl(I) was investigated using Electrochemical Impedance Spectroscopy (EIS) at both modified and unmodified electrode surfaces under optimal conditions. Fig. 8 shows the reduction in charge transfer resistance, indicating improved surface modification of the electrodes. A larger semicircle diameter is observed for the CPE. However, the semicircle diameter decreased when using rGO-Fe_3O_4/N-B-3-MITFB/CPE. This indicates that the charge transfer resistance at the electrode surface is reduced, and the charge transfer rate increases with the use of rGO-Fe_3O_4/N-B-3-MITFB/CPE. The data obtained from the electrochemical impedance studies show good agreement with the voltammetric data presented in Fig. 7 comparing the electrodes.

3.4 Optimization of analytical conditions

3.4.1 Effect of supporting electrolyte

The influence of the electrolyte on the performance of the proposed electrode was studied using various 0.01 M solutions (HNO_3, HCl, acetate buffer, and phosphate buffer), each containing 150 µM Tl(I) ion. These solutions were tested following the established procedure. Fig. 9 demonstrates that phosphate buffer at pH = 7 yielded the highest current, making it the optimal electrolyte due to minimized surface charge effects, and the buffer's excellent ionic strength and stability. Consequently, phosphate buffer (pH = 7) was chosen for subsequent measurements.

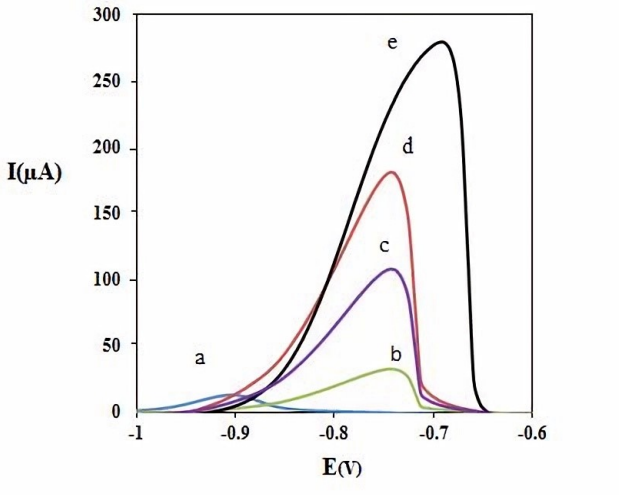

Figure 7. Differential pulse stripping voltammograms (a) rGO-Fe_3O_4/N-B-3-MITFB/CPE without the presence of Tl(I), and (b) bare CPE, (c) rGO-Fe_3O_4/CPE, (d) N-B-3-MITFB/CPE, (e) rGO-Fe_3O_4/N-B-3-MITFB/CPE in presence of 300 µM Tl(I) at a phosphate buffer (pH 7.0), respectively. Other conditions: accumulation-reduction time: 6 min, −1 V reduction potential, scan rate: 30 mV/s, pulse amplitude: 100 mV, pulse period:4 ms.

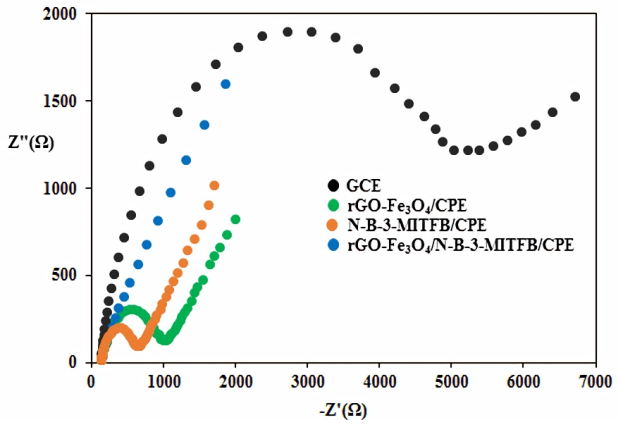

Figure 8. Nyquist plots of CPE, rGO-Fe_3O_4/CPE, N-B-3-MITFB/CPE and rGO-Fe_3O_4/N-B-3-MITFB/CPE in the presence of 300 µM Tl(I) at the optimum condition.

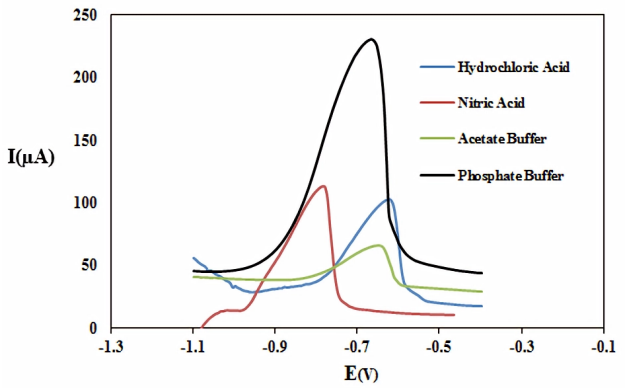

Figure 9. The effect of the type of electrolyte on the anodic peak current of rGO-Fe_3O_4/N-B-3-MITFB/CPE. Other conditions were the same as in Fig. 7 except electrolyte.

3.4.2 Effect of pH

The effect of the pH of the electrolyte solution (phosphate buffer) containing 150 µM Tl(I) ion in the range of 4.0 to 9.0 on the anodic peak current of rGO-Fe_3O_4/N-B-3-MITFB/CPE was investigated. Based on the results obtained, which are reported in Fig. 10, the highest anodic peak current is observed at pH = 7. Therefore, phosphate buffer at pH = 7 was employed in the following analyses.

3.4.3 Effect of accumulation-reduction potential and time

The effect of the reduction and accumulation potential on the Tl(I) anodic peak current was investigated in the range of −0.1 to −1.2 V using the proposed method in the presence of 150 µM Tl(I), and the results are reported in Fig. 11 (A). As can be seen, increasing the potential from −0.1 to −1 V increases the anodic peak current, with the highest current observed at −1 V due to optimal Tl(I) reduction and accumulation kinetics. At more negative potentials, the current decreases, likely due to interference from competing ion migration. Therefore, a potential of −1 V was selected as the applied potential for the reduction and accumulation of Tl(I) ions on the surface of the modified electrode. The effect of reduction time on the anodic peak current of Tl(I) was evaluated within the range of 20 to 600 seconds at a concentration of 150 µM Tl(I) (Fig. 11 B). The peak current showed a progressive increase up to 400 seconds, after which it plateaued. This increase is attributed to the accumulation and reduction of more Tl(I) ions on the electrode surface. By 400 seconds, nearly all adsorbed Tl^+ ions are converted to Tl^0. Further increases in reduction time do not increase the current due to saturation of the electrode surface. Therefore, 400 seconds was selected as the optimal reduction time.

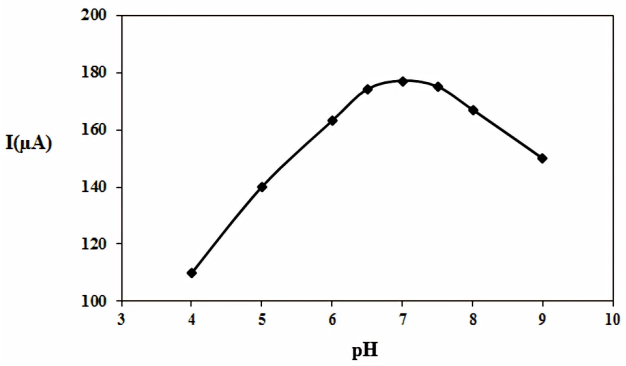

Figure 10. The effect of pH on the rGO-Fe_3O_4/N-B-3-MITFB/CPE response. Other conditions were the same as in Fig. 7 except pH.

3.5 Performance characteristics

To establish a calibration curve and determine the linear range of the proposed method, solutions with varying Tl(I) concentrations were prepared, and the anodic peak current was measured according to the proposed procedure. The calibration curve was plotted based on current versus concentration. The results obtained indicate a concentration range of 0.07 to 420 µM with a detection limit of 0.9 nM for Tl(I) (Fig. 12). The relative standard deviation (R.S.D.), which indicates the accuracy of the method, was found to be ±0.79% for seven consecutive measurements of identical samples containing 50.0 µM Tl(I). This demonstrates excellent repeatability in the modified electrode structure, likely attributed to the strong adsorption of Tl(I) on the electrode surface.

3.6 Stability and reproducibility investigation

The stability and reproducibility of the rGO-Fe_3O_4/N-B-3-MITFB/CPE were evaluated under optimized laboratory conditions. To assess reproducibility, the rGO-Fe_3O_4 nanocomposite was synthesized in three independent batches under identical conditions. For each batch, five mod-

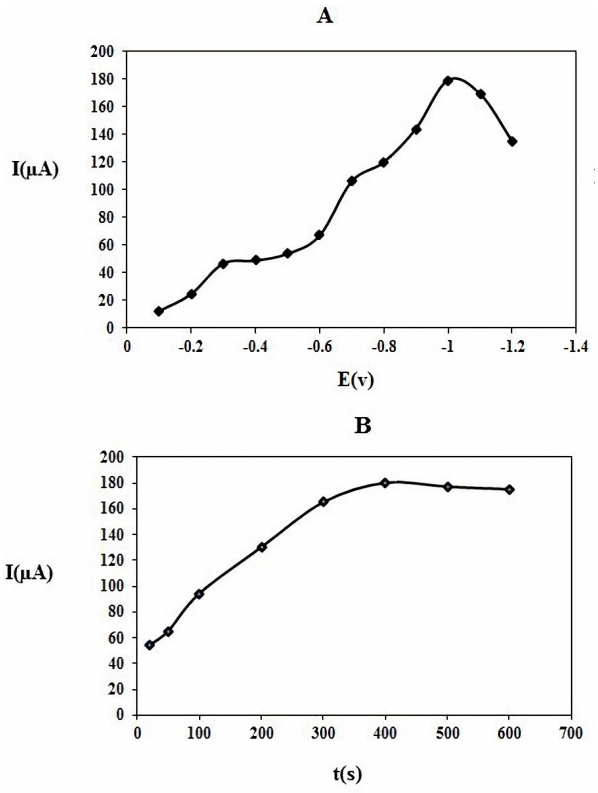

Figure 11. The effect of reduction potential (A) and time (B) on the anodic peak current of rGO-Fe_3O_4/IL/MCPE. Other conditions were the same as in Fig. 7 except reduction potential and time.

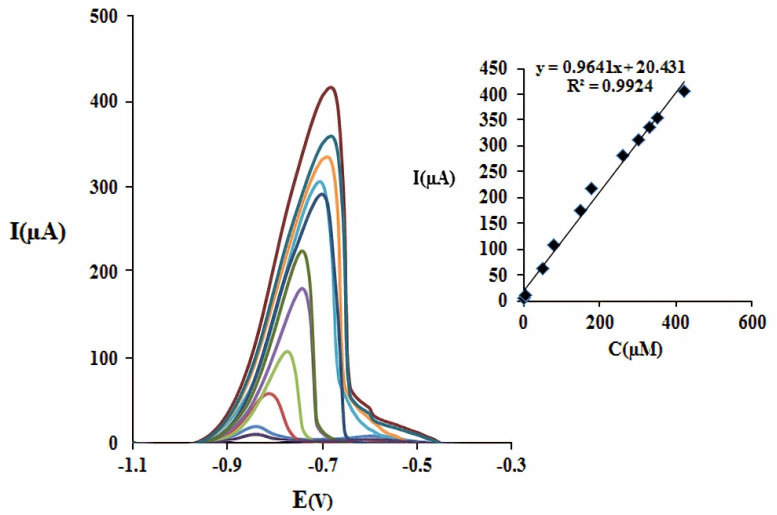

Figure 12. DPASVs of various concentrations of Tl(I) in 0.01 M phosphate buffer solution (pH 7.0) (down to up: 0.07, 3.0, 50.0, 80.0, 150.0, 180.0, 260.0, 300.0, 330.0, 350.0 and 420 μM). Inset: Linear calibration curves of the anodic peak currents vs. Tl(I) concentration.

ified electrodes were fabricated and tested under the same conditions for the measurement of a 150 μM Tl(I) solution. The relative standard deviation (RSD) for the first, second, and third batches were 2.8%, 3.1%, and 2.9%, respectively. Moreover, the inter-batch relative standard deviation (RSD) was calculated to be 3.5%, indicating that the synthesis of rGO-Fe_3O_4 is stable and reproducible, and that the performance of the modified electrodes across different batches is consistent. In addition, the intra-batch reproducibility for each batch was below 3.5%, further confirming the reliability of the electrode fabrication method. Furthermore, to evaluate operational stability, the electrode was stored under laboratory conditions and tested after 14 days. The electrode retained more than 97% of its initial response in the presence of 150 μM thallium solution, demonstrating good stability for repeated use. Additionally, the stability of the electrode in DPASV was assessed over 20 consecutive cycles under identical conditions. A gradual decrease of approximately $5-10\%$ in the peak current was observed after $15-20$ cycles. This behavior can be attributed to the porous structure of the carbon paste and the presence of nanoparticles, which together enhance the electrode's resistance to fouling. After 20 cycles, the decrease in peak current was likely due to the gradual accumulation of solution components on the electrode surface. The electrode's performance was regenerated by gentle mechanical polishing and subsequent cyclic voltammetry in 0.1 M H_2SO_4, which effectively removed surface deposits and restored the electrode response.

These results confirm the reliability of the modified electrode for routine electrochemical analysis of Tl(I) ions in aqueous samples.

3.7 Interferences study

The effect of interfering species on the measurement of Tl(I) using the proposed method was investigated in a solution containing 150 μM of Tl(I), with a maximum acceptable error of 5% in current and potential. The observations showed that no interference was observed for the analysis of Tl(I) at concentration levels of 600 times higher for Al^{3+}, Na^{+}, F^{-}, Mg^{+2}, NO_3^{-}, K^{+}, Cl^{-}, 500 times higher for folic acid, uric acid, humic acid, phenol and nitrophenol, 450 times higher for catechol, sodium dodecyl sulfate (SDS), glucose, glutamic acid, and 300 times higher for Cr^{+2}, Pb^{+2}, Ni^{+2}, Hg^{+2}, and Cu^{+2}.

3.8 Real sample analysis

The validity of the proposed procedure for the determination of Tl(I) in various water matrices, including drinking water, well water, and industrial wastewater, was assessed through the standard addition approach. As summarized in Table 1, the obtained recovery results confirm the satisfactory accuracy and applicability of the developed sensor in real-world samples.

Table 1. Determination of Tl(I) in real samples (n = 3).

Sample	Tl(I) added (μM)	Tl(I) found (μM)	Recovery (%) (Tl(I))
Drinking water[a]	-	< LOD*	-
	25.0	24.8 ± 1.2	99.2
	50.0	48.9 ± 2.3	97.5
Well water[b]	-	< LOD	-
	25.0	24.5 ± 2.1	98.0
	50.0	49.3 ± 1.4	98.6
Waste water[c]	-	7.2 ± 0.5	-
	25.0	32.8 ± 1.1	102.4
	50.0	58.1 ± 1.7	101.8

[a] Kerman drinking water, Kerman, Iran
[b] Shahid Bahonar University of Kerman, Kerman, Iran
[c] Copper factory, Sarcheshmeh, Kerman, Iran
*< LOD: below 0.9 nM.

4. Conclusion

Thallium (Tl), recognized as one of the highly toxic heavy metals, has attracted growing concern due to its detrimental impacts on human health and environmental systems, even at trace concentrations. Effective monitoring of water sources is therefore crucial to ensure both public health protection and ecological safety. In this study, a sensor modified with ionic liquid and graphene was designed to determine Tl(I) in water samples. The rGO-Fe_3O_4/N-B-3-MITFB/CPE, in combination with refined differential pulse anodic stripping voltammetry (DPASV), showed a wide concentration range ($0.07 - 420$ µM), a very good detection limit (0.9 nM), and high sensitivity and selectivity for Tl(I) measurement. Moreover, the innovative application of the nanocatalyst for Tl(I) determination in the presence of common inorganic and organic interferents has led to remarkable selectivity and stability of the proposed sensor. The successful application of this sensor in various water samples confirmed its effectiveness in monitoring Tl(I) contamination in different environmental conditions. Overall, this study contributes to the development of efficient tools for environmental monitoring and supports efforts to reduce the risks associated with Tl(I) contamination.

Authors Contribution
All authors assisted to the conceptualization, literature review, experimental work, data sample analysis, as well as writing, formatting, and editing of the manuscript.

Availability of data and materials
The data that support the findings of this study are available from the corresponding author, upon reasonable request.

Conflict of interests
The authors declare that they have no known competing financial interests or personal relationships that could have appeared to influence the work reported in this paper.

References

[1] J.J. Rodríguez-Mercado and M.A. Altamirano-Lozano. "Genetic toxicology of thallium: a review ". *Drug Chem. Toxicol.*, **36**:369–383, 2013.

[2] B. Blumenthal, K. Sellers, and M. Koval. "Thallium and thallium compounds ". *Kirk-Othmer Encycl Chem Technol.*, , 2023.

[3] J. Liu, X. Luo, Y. Sun, D.C. Tsang, J. Qi, W. Zhang, and G. Sheng. "Thallium pollution in China and removal technologies for waters: A review". *Environ. Int.*, **126**:771–790, 2019.

[4] Z. Song, H. Deng, Z. Chen, T. Liu, and T. Xiao. "Accumulation of thallium and potential toxic elements in a water-soil-rice system from a pyrite mining area, southern China: Source apportionment and health risk assessment". *J. Environ. Chem. Ecotoxicol.*, **7**:407–416, 2025.

[5] T. Wallbridge, S. James, R. Lee, A. Khan, S. Bradberry, and M.E. Elamin. "Successful treatment of potentially lethal dose thallium sulfate poisoning with sequential use of Prussian blue and multiple-dose activated charcoal ". *Clin. Toxicol.*, **61**:200–201, 2023.

[6] J. Fujihara and N. Nishimoto. "Thallium-poisoner's poison: An overview and review of current knowledge on the toxicological effects and mechanisms". *Curr Res Toxicol.*, **6**:100157, 2024.

[7] L. Osorio-Rico, A. Santamaria, and S. Galván-Arzate. "Thallium toxicity: general issues, neurological symptoms, and neurotoxic mechanisms". *Neurotoxic. Met.*, **18**:345–353, 2017.

[8] J. Wang, G. Fei, P. Zheng, N. Yan, G. Chen, W. Li, and L. Guo. "Solution Cathode Glow Discharge–Atomic Emission Spectrometry (SCGD-AES) With an Interference Filter for Spectral Discrimination for the Determination of Thallium in Surface Water ". *Anal. Lett.*, **58**:415–424, 2025.

[9] W. Liu, L. Deng, H. Li, W. Lin, Y. Yang, L. Zhang, and R. Zhu. "Determination of trace heavy metal ion Tl (I) in water by energy dispersive X-ray fluorescence spectrometry using prussian blue dispersed on solid sepiolite ". *Talanta*, **284**:127295, 2025.

[10] J. Kowalska, A. Drwal, K. Tutaj, L. Kovshun, and B. Krasnodebska-Ostrega. "On site separation of inorganic forms of thallium and arsenic in sea water systems followed by ICP-MS determination". *Anal. Methods.*, **15**:6082–6087, 2023.

[11] Y. Zhao, F. Cheng, B. Men, Y. He, H. Xu, X. Yang, and D. Wang. "Simultaneous separation and determination of thallium in water samples by high-performance liquid chromatography with inductively coupled plasma mass spectrometry ". *J. Sep. Sci.*, **42**:3311–3318, 2019.

[12] Y.L. Chu, R.Y. Wang, and S.J. Jiang. "Speciation analysis of thallium by reversed-phase liquid chromatography-inductively coupled plasma mass spectrometry". *J. Chin. Chem. Soc.*, **59**:219–225, 2012.

[13] S. Cheraghi, M.A. Taher, and H. Fazelirad. "Voltammetric sensing of thallium at a carbon paste electrode modified with a crown ether ". *Mikrochim. Acta.*, **180**:1157–1163, 2013.

[14] X. Jin, M. Baghayeri, M. Nodehi, M.S. Koshki, A. Ramezani, M. Fayazi, and P. Makvandi. "Evaluation of thallium ion as an effective ion in human health using an electrochemical sensor". *Environ. Res.*, **238**:117026, 2023.

[15] R. Wu, J. Zou, L. Deng, C. Gu, W. Lin, Z. Huang, and R. Zhu. "Prussian Blue Nanoparticle-Modified Glassy Carbon Electrode for Electrochemical Determination of Thallium (I)". *J. Anal. Chem.*, **79**:1624–1634, 2024.

[16] S. Baweja, A. Lochab, S. Baxi, and R. Saxena. "Computational investigation of thallium interactions with functionalized multi-walled carbon nanotubes for electrochemical sensing applications". *Pure Appl. Chem.*, **96**:421–428, 2024.

[17] D. Melucci, S. Casolari, M. Locatelli, and C. Locatelli. "Thallium: A Polluting Metal of New Generation. Its Voltammetric Determination in Herbal Medicines in Presence of Metal Interferences". *Analytica*, **2**:76–83, 2021.

[18] P. Inaudi, C. Esposito, M. Malandrino, L. Favilli, A. Giacomino, and O. Abollino. "Development of a portable method for monitoring and speciation of arsenic in aquatic systems by anodic stripping voltammetry: Applications to real samples ". *Talanta*, **291**:127880, 2025.

[19] Y. Yang, Y. Huang, H. Luo, J. Zhao, J. Bi, and G. Wu. "Ion interference and elimination in electrochemical detection of heavy metals using anodic stripping voltammetry". *J. Electrochem. Soc.*, **170**:057507, 2023.

[20] J. Zhang, S. Wu, Z. Wu, F. Zhang, B. Jin, and C. Yang. "Review of Underwater In Situ Voltammetry Analyzers for Trace Metals". *Chemosensors*, **12**:158, 2024.

[21] S. Cheraghi, M. A Taher, M. Bijad, and H. Sadeghifar. "A review: Stripping voltammetric methods as a high sensitive strategy for trace analysis of ions, pharmaceutical and food samples". *Curr. Anal. Chem.*, **13**:5–12, 2017.

[22] J. Barón-Jaimez, M.R. Joya, and J. Barba-Ortega. "Anodic stripping voltammetry–ASV for determination of heavy metals ". *J. Phys. Conf. Ser.*, **466**:012023, 2013.

[23] A. Joseph, S. Subramanian, P.C. Ramamurthy, S. Sampath, R.V. Kumar, and C. Schwandt. "Iminodiacetic acid functionalized polypyrrole modified electrode as Pb (II) sensor: synthesis and DPASV studies ". *Electrochim. Acta*, **137**:557–563, 2014.

[24] P. Sengupta, K. Pramanik, and P. Sarkar. "Simultaneous detection of trace Pb (II), Cd (II) and Hg (II) by anodic stripping analyses with glassy carbon electrode modified by solid phase synthesized iron-aluminate nano particles ". *Sensor. Actuators. B. Chem.*, **329**: 129052, 2021.

[25] S. Eloul and R.G. Compton. "Voltammetric sensitivity enhancement by using preconcentration adjacent to the electrode: simulation, critical evaluation, and insights". *J. Phys. Chem. C.*, **118**:24520–24532, 2014.

[26] K. Wang, R. Liang, and W. Qin. "Enhancing the sensitivity of polymeric membrane polycation-sensitive electrodes by surface modification of a polydopamine nanolayer". *Sensor. Actuat. B. Chem.*, **405**:135310, 2024.

[27] I. Tomac, V. Adam, and J. Labuda. "Advanced chemically modified electrodes and platforms in food analysis and monitoring". *Food Chem.*, **460**:140548, 2024.

[28] S. Cheraghi, F. Shalali, and M.A. Taher. "Kojic acid exploring as an essential food additive in real sample by a nanostructure sensor amplified with ionic liquid". *J. Food Meas. Charact.*, **17**.

[29] A. Cetinkaya, S.I. Kaya, M. Yence, F. Budak, and S.A. Ozkan. "Ionic liquid-based materials for electrochemical sensor applications in environmental samples". *Trends Environ. Anal. Chem.*, **37**:e00188, 2023.

[30] J. Pereira, R. Souza, and A. Moita. "A Review of Ionic Liquids and Their Composites with Nanoparticles for Electrochemical Applications ". *Inorg.*, **12**:186, 2024.

[31] M.A. Raj and S.A. John. "Graphene-modified electrochemical sensors". *Graphene-Based Electrochemical Sensors for Biomolecules.*, : 1–41, 2019.

[32] Z. Hsine, R. Mlika, N. Jaffrezic-Renault, and H. Korri-Youssoufi. "Recent progress in graphene based modified electrodes for electrochemical detection of dopamine". *Chemosensors*, **10**:249, 2022.

[33] N.Z.M. Azman, P.N.S. Zainal, and S.A. Alang Ahmad. "Enhancement the electrochemical conductivity of a modified reduced graphene oxide/calixarene screen-printed electrode using response surface methodology". *Plos one*, **15**:e0234148, 2020.

[34] F. Yusoff, K. Suresh, W.M. Khairul, and M.S. Noorashikin. "Electrocatalytic Reduction of Oxygen on Reduced Graphene Oxide/Iron Oxide (rGO/Fe_3O_4) Composite Electrode". *Russ. J. Phys. Chem. A.*, **95**:834–842, 2021.

[35] J.S. Niranjana, H. Koyakutty, A.A. Thomas, and M.J. Bushiri. "Novel synthesis of multi-layered rGO/Fe_3O_4 nanocomposite in a single step and its efficient electrochemical sensing of vitamin C". *Mater. Sci. Eng. B.*, **290**:116283, 2023.

[36] A. Elgamouz, A.N. Kawde, I.A. Shehadi, S. Sayari, S.A. Abdullah Mohammed, A. Abdelrazeq, and K. Hasan. "Modified graphite pencil electrode based on graphene oxide-modified Fe_3O_4 for ferrocene-mediated electrochemical detection of hemoglobin ". *ACS omega.*, **8**:11880–11888, 2023.

[37] S. Mutić, J. Anojčić, M. Vranes, J. Panić, and S. Papović. "Voltammetric determination of organic UV filters by carbon paste electrodes modified with pyridinium-based ionic liquids". *Talanta*, **266**:125103, 2024.

[38] S. Upasham, I.K. Banga, B. Jagannath, A. Paul, K.C. Lin, S. Muthukumar, and S. Prasad. "Electrochemical impedimetric biosensors, featuring the use of Room Temperature Ionic Liquids (RTILs): Special focus on non-faradaic sensing". *Biosens. Bioelectron.*, **177**:112940, 2021.

[39] R. Rama, S. Meenakshi, K. Pandian, and S.C.B. Gopinath. "Room temperature ionic liquids-based electrochemical sensors: an overview on paracetamol detection". *Crit. Rev. Anal. Chem.*, **52**:1422–1431, 2022.

[40] Z. Zhang, H. Zheng, Y. Liu, S. Ma, Q. Feng, J. Qu, and X. Zhu. "Highly sensitive detection of multiple antiviral drugs using graphitized hydroxylated multi-walled carbon nanotubes/ionic liquids-based electrochemical sensors". *Environ. Res.*, **249**:118466, 2024.

[41] L. Oularbi, M. Turmine, F.E. Salih, and M. El Rhazi. "Ionic liquid/-carbon nanofibers/bismuth particles novel hybrid nanocomposite for voltammetric sensing of heavy metals ". *J. Environ. Chem. Eng.*, **8**: 103774, 2020.

[42] H. Karimi-Maleh, M. Shafieizadeh, M.A. Taher, F. Opoku, E.M. Kiarii, P.P. Govender, and Y. Orooji. "The role of magnetite/graphene oxide nano-composite as a high-efficiency adsorbent for removal of phenazopyridine residues from water samples, an experimental/theoretical investigation ". *J. Mol. Liq.*, **298**:112040, 2020.

[43] D.C. Marcano, D.V. Kosynkin, J.M. Berlin, A. Sinitskii, Z. Sun, A. Slesarev, and J.M. Tour. "Improved synthesis of graphene oxide.". *ACS Nano.*, **4**:4806–4814, 2010.

[44] S. Petnikota, H. Maseed, V.V.S.S. Srikanth, M.V. Reddy, S. Adams, M. Srinivasan, and B.V.R. Chowdari. "Experimental elucidation of a graphenothermal reduction mechanism of Fe_3O_4: An enhanced anodic behavior of an exfoliated reduced graphene oxide/Fe_3O_4 composite in Li-ion batteries.". *J. Phys. Chem. C.*, **121**:3778–3789, 2017.

[45] S. Gürsoy, N.K. Zeytinci, B.T. Zaman, S. Bakırdere, and E. Öztürk Er. "Study of linear and nonlinear isotherm and kinetic parameters of hexavalent chromium adsorption onto reduced graphene oxide coated iron oxide". *Sci. Rep.*, **15**:25206, 2025.